



1 Improvement of Soil Properties Maps using an Iterative Residual Correction Method 2 Chengcheng Xu<sup>1</sup>, Elia Scudiero<sup>23</sup>, Ray Anderson<sup>32</sup>, Nathaniel Chaney<sup>1</sup> 3 <sup>1</sup> Department of Civil and Environmental Engineering, Duke University, Durham, NC 27705, 4 USA 5 <sup>2</sup> Department of Environmental Sciences, University of California Riverside, Riverside, CA 6 92521, USA 7 <sup>3</sup> United States Department of Agriculture – Agricultural Research Service, George E. Brown 8 Jr. Salinity Laboratory, Agricultural Water Efficiency and Salinity Research Unit, Riverside, 9 CA 92507, USA 10 Correspondence to: Chengcheng Xu (Chengcheng.xu@duke.edu) 11 12 **Short Summary** 13 Accurate soil information is important. This study developed a new method that improves 14 existing soil maps by correcting their probability distributions using newly collected soil 15 measurements. By repeatedly adjusting previous predictions, the method makes soil 16 maps more accurate and more certain. The application in California improved the 17 performance of predictions for soil texture, organic matter, and bulk density. This method 18 can be further used for more soil properties and regions. 19 20 **Abstract** 21 Accurate mapping of soil properties is vital for many applications including precision

irrigation and fertilization. However, existing models for digital soil maps underestimate

https://doi.org/10.5194/egusphere-2025-5107 Preprint. Discussion started: 21 November 2025 © Author(s) 2025. CC BY 4.0 License.



23

24

25

26

27

28

29

30

31

32

33

34

35

36

37

38

39

40

41

42

43

44



their spatial variability or prediction uncertainties, which introduces risk for applications including agricultural irrigation and fertilization. This study introduces a hybrid approach that combines prior soil predictions with iterative residual correction to improve soil mapping performance using a Californian case study to demonstrate its application. We first generate prior probabilistic soil property maps using a pruned hierarchical Random Forest (pHRF) method. These prior estimates are then refined by integrating additional soil profile data and iteratively adjusting residuals of distribution of soil properties (differences between observation and prior predictions) pixel by pixel. It gradually adjusts the statistical shape of soil property distributions and incrementally corrects bias of prior knowledge with observed soil information. We evaluated soil mapping over California and at 1-km resolution to test the methodology. For residual correction, we compiled laboratorymeasured soil profile data from three primary sources: the World Soil Information Service (WoSIS), the National Soil Characterization Database (SCD), and field measurements conducted by the University of California, Riverside (UCR) and the USDA-ARS United States Salinity Laboratory. From the evaluations, the posterior soil texture predictions show an RMSE of less than 10%, a 7% reduction compared to the priors (pHRF-derived soil maps). For soil organic matter (SOM) and oven-dry bulk density (BD), the RMSE also decreased, as the priors initially underestimated their spatial variation. Although posterior SOM and BD predictions were less accurate than other soil properties, this was expected since they are dynamic soil properties and their response to environment and anthropogenic activities is more difficult to simulate. The residual correction also showed reduced uncertainties, as demonstrated by narrower prediction intervals compared to the





45 priors. This method also applied optimization with physical constraints, such as ensuring 46 the bounds of soil property values. This study presents a two-step framework that 47 improves accuracy and reduces uncertainty for DSM applications. 48 49 1 Introduction 50 Soils play an important role in regulating Earth's water, energy, and nutrient cycles 51 (Vereecken et al., 2016). Soil maps guide agricultural practices, ecosystem management, 52 hydraulic modeling, and climate studies, such as crop modeling, flood risk assessment, 53 groundwater management, and climate change (Vereecken et al., 2022). The importance 54 of soil maps has increased with the advent of precision agriculture, including site-specific 55 seeding, irrigation, and fertilization recommendations that intrinsically depend on highresolution soil properties (Jiang et al., 2011; Li et al., 2019; Mueller et al., 2001; Ortuani et 56 57 al., 2016). However, the accuracy and reliability of these management actions heavily 58 depend on the quality of soil maps as a critical decision-making input. Traditional soil 59 surveys involve field observations, laboratory analyses, and expert interpretation, but are 60 labor-intensive and expensive (Grunwald et al., 2011; Rossiter et al., 2022; Soil Survey Staff 61 et al., 2023). These limitations have driven the development of digital soil mapping (DSM) 62 techniques. DSM leverages decades of soil data collection and sharing, establishing 63 quantitative models to generate georeferenced soil maps. 64 65 Digital soil maps are typically derived from existing soil surveys, geostatistical models, 66 machine learning, or hybrid approaches. Soil survey-based soil mapping method, which





68

69

70

71

72

73

74

75

76

77

78

79

80

81

82

83

84

85

86

87

88

use low, high, and representative values to describe soil property distributions for each soil component (Soil Survey Staff et al., 2023). The method typically approximates each soil component as a triangular distribution (Chaney et al., 2016; Soil survey staff, 2023), potentially oversimplifying multi-modal distributions of soil properties in some cases (Haghverdi et al., 2020; Nussbaum et al., 2023). Additionally, estimating soil properties from synthetic sampling within a map unit could create artificial spatial patterns, adding noises into the mapping results (Chaney et al., 2019). Developments such as hyper-Latin sampling and landscape adaptive covariance functions have improved the representation of spatial patterns of soil properties (Minasny and McBratney, 2006). Yet, soil surveybased approaches remain valuable particularly in areas where soil profile data is limited (Nauman et al., 2024). Geostatistical models, which rely on expert knowledge and assumed spatial correlation functions, are often difficult to apply in areas with insufficient field knowledge (Oliver and Webster, 2014). To address these challenges, non-parametric models, such as Random Forest, trained with hybridized soil data that combine soil surveys with georeferenced soil profiles show potentials in improving soil mapping, particularly for large-scale maps (Nauman et al., 2024). Map of soil properties have been observed with bias compared to field observations in certain areas due to many factors (Hengl et al., 2017; Powers et al., 2011). At the measurement level, sampling methods may favor certain landscape positions or soil conditions, causing a clustered representation (Ramcharan et al., 2018). In areas with coarse sampling density, models trained on unrepresentative data are likely to deviate





90

91

92

93

94

95

96

97

98

99

100

101

102

103

104

105

106

107

108

109

110

from actual observations (Sharififar et al., 2019). Commonly used DSM models can show bias. For example, Random Forest classifier favors the majority class (Chen et al., 2004), and Random Forest regressors struggle to capture extreme values (Nauman et al., 2024). Furthermore, certain areas may not be fully captured by the DSM model and the selected feature space, such as areas with complex glacial pattern, parent material transitions, and alluvial processes (unaddressed problem in SOLUS; SoilGrids 2.0; (Nauman et al., 2024; Poggio et al., 2021)). Model-based solutions include using ensemble models to enhance accuracy compared to a single model (Sylvain et al., 2021). Post-processing methods, such as regression kriging and bias-corrected decision trees, can also be used (Hengl et al., 2004). Yet, kriging-based methods have limitations in areas with high spatial heterogeneity and abrupt transitions, where stationary assumptions do not meet. Nonparametric models can be used for bias correction that overcome the limitation of making presumed distributions. Quantifying uncertainties in DSM is important for its practical applications (Schmidinger and Heuvelink, 2023). DSM products represent soil properties as multi-dimensional matrices showing vertical and horizontal soil variation (Vereecken et al., 2022), with each pixel containing weighted possible values and their prediction uncertainties. These uncertainties can be represented either as continuous values through prediction intervals or as discrete classifications with associated class probabilities (Chaney et al., 2016, 2019; Hengl et al., 2017; Ramcharan et al., 2018). Common quantification approaches include geostatistical techniques like kriging, where the nugget term accounts for





112

113

114

115

116

117

118

119

120

121

122

123

124

125

126

127

128

129

130

131

132

measurement errors while kriging variance reflects spatial uncertainty patterns (Chilès and Delfiner, 2012; Takoutsing et al., 2022), and machine learning methods such as Quantile Random Forest (QRF) which generates probability distributions from decision tree outputs using values of soil properties (Poggio et al., 2021; Shi et al., 2024). For discrete classifications, uncertainty derives from soil raster probabilities during soil taxa classification (Chaney et al., 2016; Odgers et al., 2015). Given the data-driven nature of DSM and frequent limitations in soil profile availability, integrating multiple qualified data sources improve the amount of soil data and reduce prediction uncertainties (Nauman et al., 2024), particularly in regions where predictions must rely more heavily on legacy soil data. Using soil raster probabilities can utilize existing soil taxonomy information from soil surveys while also leverage soil profiles to correct bias for prior predictions. In this study, we present a hybrid DSM approach combining pruned Hierarchical Random Forest (pHRF) predictions with residual correction. The pHRF method leverages NCSS soil survey data and georeferenced soil taxa information to generate prior distributions, while additional soil profiles correct biases in posterior predictions. This method builds on development in previous research while addressing specific limitations. Sylvain et al. (2021) applied XGBoost (sequential decision trees) and ensemble models to correct deterministic soil property maps, demonstrating reduced bias for many soil properties (Sylvain et al., 2021). Zhang et al. (2010) introduced a bias-correction technique with Random Forest models to mitigate their tendency to regress toward mean values, though not in DSM contexts (Zhang and Lu, 2012). Our approach extends these concepts by



© **()** 

probabilistically updating posterior distributions at each location through an iterative correction process that continues until convergence across vertical intervals. Vertical correlations are maintained through layer-by-layer residual correction, which preserves inter-layer correlations while dynamically optimizing the feature space at each correction step. Unlike methods requiring distributional assumptions, our non-parametric framework adapts to diverse landscapes and data scenarios. The models implement residual correction by minimizing the differences between priors and new observed to adjust posterior distributions, with the entire process continuing until property variations stabilize between iterations. This method aims to improve the accuracy and reliability of soil property maps, supporting decision-making in relevant applications.

## 2 Methods

This study introduces a hybrid approach for DSM, combining prior soil property estimates derived from the pruned hierarchical Random Forest (pHRF) method followed with an iterative residual correction (IRC). The method integrates additional soil profiles to adjust the distribution of prior estimates, correcting biases and improving the accuracy of soil property predictions. The following sections describe the workflow of the pHRF method, the steps for residual correction, and the generation of updated posterior soil property maps.





#### 2.1 Soil Data

To correct the residuals as post processing, we only use georeferenced soil profiles with laboratory measurements of soil properties. We compiled soil profile data from three primary sources: the World Soil Information Service (WoSIS), the National Soil Characterization Database (SCD), and field measurements conducted in California. During preprocessing, we harmonized all soil data, which was originally reported at different soil horizons, into standardized depth intervals. Location of soil profiles and their distribution of soil property values are presented in Figure 1. Six soil properties are studied—sand content, silt content, clay content, pH, soil organic matter (log-scaled), and bulk density.

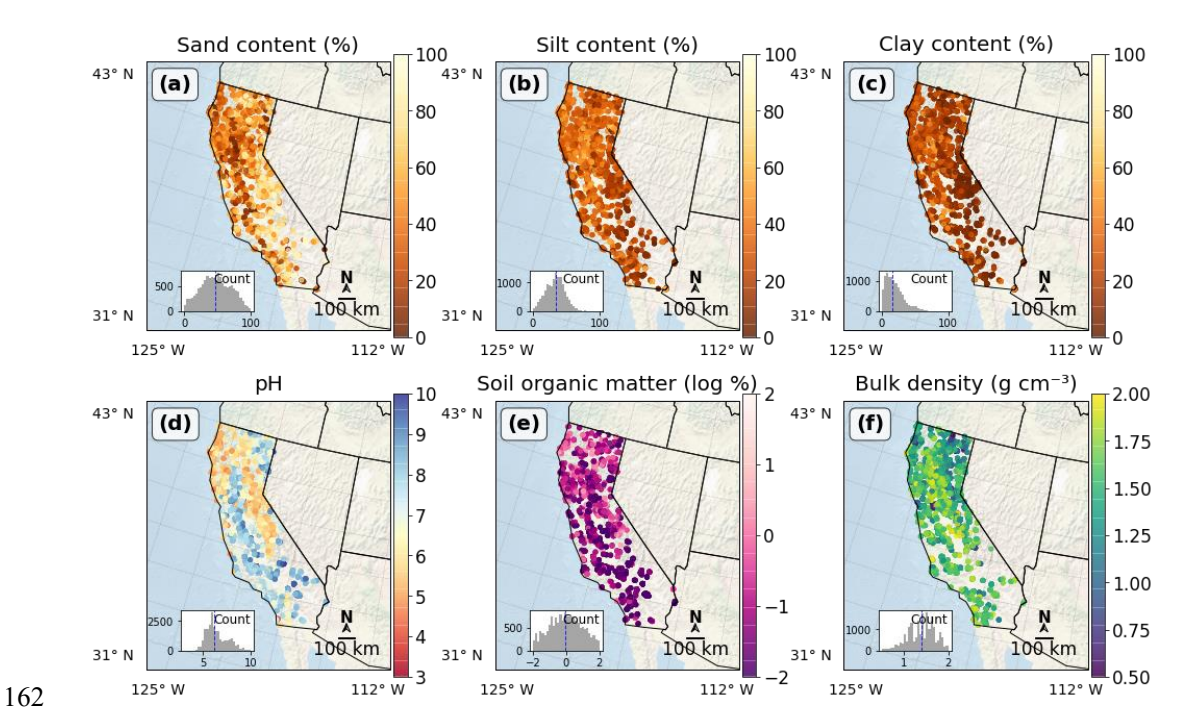


Figure 1: Spatial distribution and statistical characteristics of soil properties observations across California. The figure presents six soil parameters mapped using an Albers Equal Area projection: (a) sand content (mass %), (b) silt content (mass %),





166 (c) clay content (mass %), (d) pH, (e) soil organic matter (log-scaled mass %), and (f) 167 bulk density (g/cm<sup>3</sup>). Each subplot displays sample locations as colored points. 168 Distribution histograms in the lower left corner of each subplot show the frequency 169 distribution of values, with blue dashed lines indicating median values. Distance 170 scale bar and compass rose are provided in the right corner. 171 172 2.1.1 World Soil Information Service (WoSIS) 173 The World Soil Information Service (WoSIS), managed by the International Soil Reference 174 and Information Centre (ISRIC), aggregates global soil data from diverse sources, including 175 national soil institutes, research organizations, and collaborative initiatives like the Global 176 Soil Partnership (GSP) and the International Network of Soil Information Institutions (INSII). 177 The database provides soil properties for multiple depth intervals, georeferenced in 178 decimal degrees (WGS84), and undergoes quality controls (Batjes et al., 2024). In 179 California, WoSIS typically offers 2,000 to over 5,000 soil observations for soil property of 180 interest. Samples below 1-meter depth are fewer than those from shallower layers. 181 182 2.1.2 Soil Characterization Database (SCD) 183 The Soil Characterization Database (SCD) is a subset of the National Cooperative Soil 184 Survey (NCSS) database (National Cooperative Soil Survey, 2018). It records soil properties 185 for each soil horizon within a soil profile (pedon), including soil texture, bulk density, water 186 retention. The data are collected using standardized laboratory methods. In California, 187 SCD provides between 500 and over 1,000 soil samples per layer for the studied soil





properties. Each soil profile is georeferenced (WGS84) and includes metadata such as site location, land use, and sampling methods.

### 2.1.3 Ground truth soil sampling and measurements

Additional soil sampling was conducted to complement georeferenced soil profiles in California for model training and evaluation. These data are reported in Scudiero et al. (2024) and are briefly discussed here. Multiple fields located between Salinas and Soledad in California's Salinas Valley were selected to collect soil particle size fraction data (Figure 2). These fields, presented as red dots in Figure 2, were chosen because they were accessible, unfarmed during the sampling period, and spread across different parts of the valley.

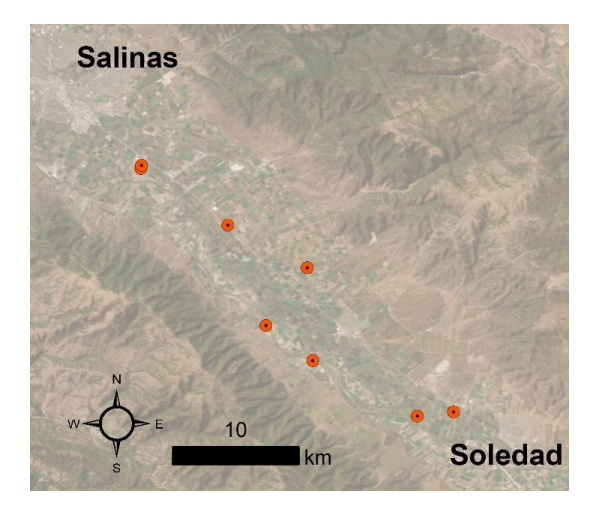


Figure 2: Map of sampling fields in the Salinas Valley in California. Each red dot represents a sampling field between Salinas and Soledad. Scale bar and direction indicator are provided in the left corner. Basemap: Environmental Systems Research





Institute (Esri) World Imagery, with imagery and data provided by Esri, Maxar, 203 204 Earthstar Geographics, and the GIS User Community. 205 206 Soil apparent electrical conductivity (ECa) was measured across fields using an 207 electromagnetic induction (EMI) sensor connected to a GPS receiver. Following the ECa-208 directed soil sampling protocols of Corwin and Scudiero (Corwin and Scudiero, 2020), the 209 most representative soil samples were identified with ESAP software package and the 210 Response Surface Sampling Design algorithm (Lesch et al., 2000; Lesch, 2005). 0-0.8 and 211 0-1.6 m soil profiles were further analyzed and followed with the expectation that ECa was 212 a regional proxy for the field-scale variability of particle size fraction. 213 214 To measure particle size fraction, soil samples were then collected from multiple depths 215 (0-0.1, 0.1-0.4, and 0.4-1.2 m) across fields. After collection, the samples were air-dried, 216 ground, and sieved to remove particles larger than 2 mm; and then measured using the 217 Integral Suspension Pressure method (The improved integral suspension pressure method 218 (ISP+) for precise particle size analysis of soil and sedimentary materials; Wolfgang Durner, Sascha C. Iden) using PARIO™ system (METER Group AG, Munich, Germany). 219 220 221 2.2 Residual Correction in DSM 222 Residual correction is implemented to address underestimated soil properties variation 223 (underestimate high values and overestimate low values). By applying residual correction 224 in post processing, we aim to improve the performance of resulting soil maps and address 225 the issue of bias in prior predictions. The schematic workflow is shown in Figure 3. There





are three primary steps in the residual correction method (1) generating prior soil properties maps, (2) preparing residuals correction, and (3) performing iterative residual correction. Details are further explained in subsections.

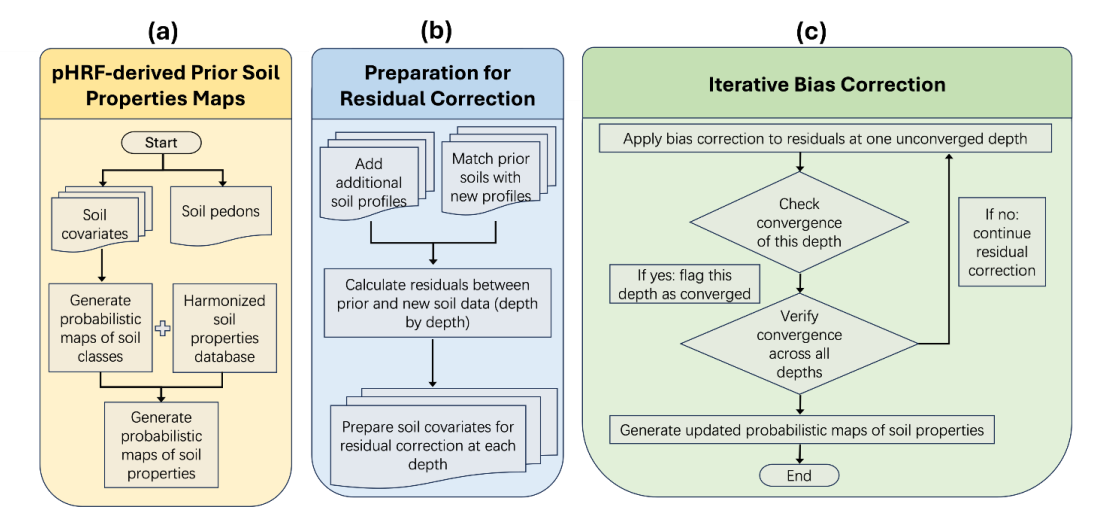


Figure 3: Workflow for updating posterior soil properties maps. The process begins with panel (a), the preparation of soil covariates and pedons to generate probabilistic maps of soil classes and properties. As illustrated in panel (b), the preparation for residual correction involves adding additional soil profiles, matching prior soils with new profiles, calculating residuals depth by depth, and preparing soil covariates for residual correction. Finally, as shown in panel (c), the iterative residual correction step applies corrections across different depths, focusing on layers where residuals have not yet stabilized. During each iteration, the model predicts residuals for one depth at a time, randomly selecting an unstable layer. Once residuals for a given depth converge, that layer is excluded from further updates, allowing the model to concentrate on remaining depths until all achieve stability. After verifying



242

243

244

245

246

247

248

249

250

251

252

253

254

255

256

257

258

259

260

261

262



convergence across all depths, the algorithm updates the posterior distribution of soil

properties and produces the final soil maps.

#### 2.2.1 Prior Soil Properties

Prior soil properties maps were generated using a pruned hierarchical Random Forest (pHRF) methodology (Xu et al., 2025). Figure 3A illustrates the workflow of the pHRF method. The DSM method begins by integrating soil covariates and soil pedons with taxonomic names to generate probabilistic maps of soil classes. These maps are then linked to a harmonized soil properties database (Chaney et al., 2019), which estimates the distribution of soil properties linked to each soil component. By combining these inputs, the pHRF method produces probabilistic maps of soil properties, serving as the prior distributions for subsequent residual correction. The pHRF method implements several key features: (1) it efficiently incorporates soil covariates such as Sentinel-1 and Sentinel-2 satellite data, GOES land surface temperature, to capture detailed land heterogeneity; (2) it uses a "moving polygon" algorithm to preserve natural landscape boundaries, ensuring spatial consistency; (3) it integrates soil pedons and soil surveys with soil properties estimates (harmonized soil properties database) to increase the availability of soil information; and (4) it employs a hierarchical structure in soil classification and pruned less plausible prediction that sharpens the prediction interval of prediction and reduces uncertainties in soil property estimates (Xu et al., 2025). The method addresses data imbalances, such as unevenly distributed soil observations and underrepresented soil classes. While the pHRF-derived soil property maps have demonstrated effectiveness in



264

265

266

267

268

269

270

271

272

273

274

275

276

277

278

279

280

281

282

283

284



reducing uncertainties, certain properties, such as bulk density, still exhibit bias (Xu et al., 2025). This shows the need for further calibration. The pHRF method produces probabilistic maps of soil properties. Each pixel contains prior distribution of soil property values and their weights. 2.2.2 Updating Posterior Soil Properties Maps Updating the posterior soil properties maps involves correcting prior soil property estimates by incorporating additional soil profiles and correcting the residuals (the differences between observed values and prior predictions). The process begins with the preparation for residual correction (Figure 3B) — calculating residuals between additional soil profiles and co-located prior soil data depth by depth. By adding these residuals to the prior distributions, the statistical shape of the probability distribution is adjusted (updated property; UP). Non-parametric model Random Forest regressors are selected for the adjustments, as they can flexibly adapt to changes in the distribution shape without relying on predefined assumptions. Additionally, soil covariates are prepared for residual correction at each depth as feature space for predictive models. The iterative residual correction method is further explained in Figure 4. Figure 4A shows a 3×3×3 matrix (latitude, longitude, and depth interval) indicating prior distributions from randomly selected spatial points A and B, where additional soil profiles are located. Depth 2 (D2; 5-15 cm) is randomly selected to initiate the process. Figure 4B details the iterative

optimization of the feature space, where weights and residuals at pixels A and B are





286

287

288

289

290

291

292

293

294

295

296

297

298

299

300

301

302

303

304

305

probabilities.

calculated and updated iteratively. Figure 4C demonstrates the iterative residual correction process, where residuals are added to the prior values to update the soil property estimates until convergence is achieved. Convergence is defined as when the median difference between updated and previous residuals falls below a predefined threshold (customizable and dependent on the soil property of interest). The final posterior soil properties are obtained by adding the last converged residuals to the prior soil property values, generating updated posterior soil property maps. 2.2.2.1 Iterative Optimization of Feature Space The feature space builds on the covariates used in the pHRF method and additional features that capture vertical correlations and intra-pixel variations of soil properties. These features include (Figure 4B): (1) Soil covariates used in the pHRF methods: these capture spatial variations in soilforming factors. Most are remote sensing data. (2) Depth information: median values of the soil horizon interval for this layer, describing the vertical variation of soil properties. (3) Representative soil property values (expected values): predicted values for each pixel in the layer, representing the most probable soil property estimates. (4) Top-probable soil properties values: current predictions at each pixel, reflecting soil heterogeneity (both intra and inter-pixel variation) and their associated





307

308

309

310

311

312

313

314

315

316

317

318

319

320

321

322

323

324

325

326

327

(5) Residuals between the target layer and other layers: difference in top-probable predicted soil property values between layers, capturing vertical correlations and aiding in the estimation of spatial patterns. To capture incremental adjustments to previous predictions, the feature space is iteratively optimized and interacted. In each iteration, residuals between soil observation and current updated predictions (UP) are added, aiming to align predictions with the observed distribution of soil properties. By updating residuals layer by layer and iteratively refining the feature space, the next prediction retains prior knowledge while integrating new information (soil heterogeneity and correcting bias; (Wu et al., 2025)). In addition, the iterative optimization of feature space captures depth-specific information and vertical relationships through feature interaction and improves potential inefficient training inherent from previous predictions. 2.2.2.2 Convergence of Residual Correction Residuals (or biases), defined as the differences between observed soil property values and current predictions, are iteratively calculated and added to the previous predictions. Previous predictions refer to predicted soil property values from a previous iterative residual correction, while prior values refer to the pHRF-derived soil property values. During each iteration (Figure 4C), residuals are computed for a specific depth layer and used to adjust the predictions. The updated predictions are then re-evaluated to determine

if further adjustments are needed, focusing on one layer at a time.





The residual correction process continues until the median difference between updated residuals and previous residuals falls below a predefined threshold. Convergence is achieved when the residuals stabilize across multiple iterations, indicating that further adjustments do not significantly change the predictions. This stability ensures that the final posterior soil properties are reliable and consistent. The stopping criteria is a customizable parameter. In this work, it was set to be 5<sup>th</sup> percentile of distribution of value changes. To avoid over-correcting bias (overfitting), only the last converged residuals are added to the prior prediction to generate the final posterior results. This method also addresses evaluation bias by achieving convergence across multiple iterations.

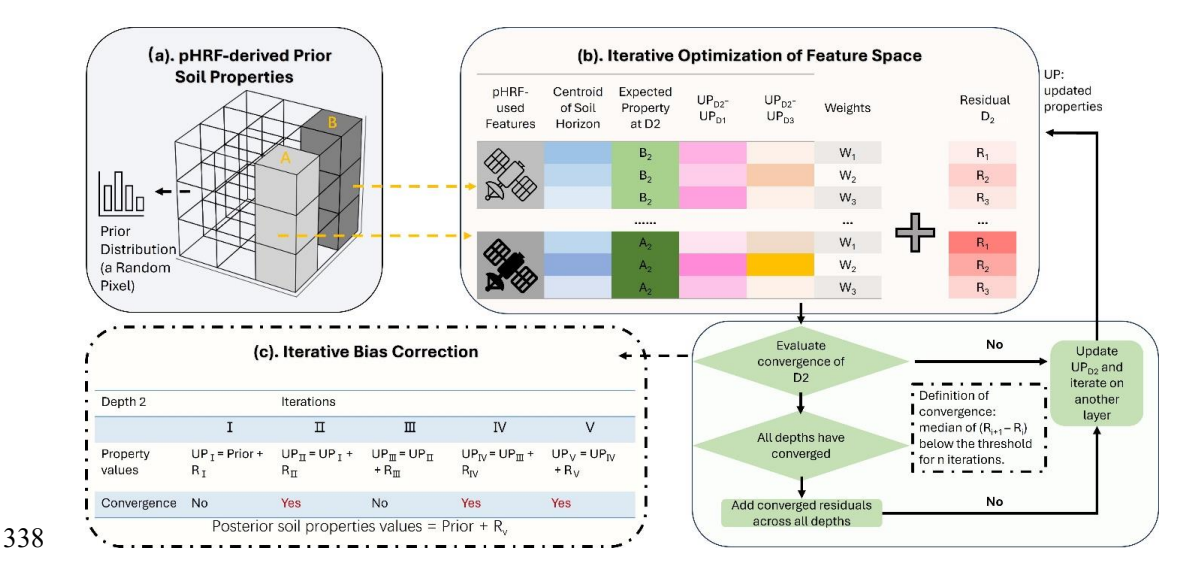


Figure 4: Schematic workflow of iterative residual correction (IRC) for Soil Properties. The workflow have three main components: (a) prior soil properties derived from the pruned hierarchical Random Forest (pHRF) method, (b) iterative optimization of the feature space, where  $W_1, W_2, W_3$  represent weights assigned to soil





properties at each pixel;  $R_1, R_2, R3$  represent possible residuals at each pixel (observed minus predicted soil property values); and  $R_{i+1}$  and  $R_i$  indicate updated and previous residuals, respectively;  $A_2$  and  $B_2$  in the table of feature space indicate that the expected value remains the same for each pixel; while colored cells indicate intravariation within each pixel. And (c) iterative residual correction and convergence check, where  $UP_1$  to  $UP_v$  represent updated property values in each iteration for a specific layer; and  $R_i$  to  $R_v$  are their associated residuals values. Convergence is achieved when the median difference between updated ( $R_{i+1}$ ) and previous ( $R_i$ ) residuals falls below a predefined threshold. The final posterior soil properties are obtained by adding the last converged residuals to the prior values.

### 2.2.2.3 Optimization with Constraints

During residual correction, a common issue arises where the addition of residuals to prior soil property values results in values that exceed physical bounds (such as sand content > 100%). To address this, an optimization process with constraints is implemented. During the first iteration, residuals are first computed without constraints. The updated soil property values are then examined to ensure they fall within predefined bounds (such as 0% to 100% for particle size fractions). If a value exceeds the bounds, it is adjusted to the nearest bound (minimum or maximum), and the remaining residuals are redistributed to other bins. This ensures that the total residuals remain consistent with the expected values while maintaining physical plausibility. This constrained optimization approach guarantees that the final posterior soil property maps are physically realistic. In addition,





365 particle size fractions are treated as compositional data, ensuring their sum is 100% at 366 each pixel. 367 368 3 Results 369 The iterative residual correction method is applied to pHRF-derived prior soil properties, 370 including particle size fractions (sand, silt, clay), pH, oven-dry bulk density (BD), and soil 371 organic matter (SOM). This correction addresses biases in the prior soil property maps and 372 updates the posterior distributions of these properties. These soil properties are important 373 for land management and serve as essential inputs for pedotransfer functions. The 374 residual correction is performed across California, covering six depth intervals: 0-5 cm, 5-375 15 cm, 15-30 cm, 30-60 cm, 60-100 cm, and 100-200 cm. 376 377 3.1 Performance Evaluation of Posterior Soil Properties 378 Table 1 presents the performance metrics for the posterior predictions of six key soil 379 properties: sand, silt, clay, pH, oven-dry bulk density (BD), and soil organic matter (SOM). 380 The metrics include the root mean square error (RMSE), coefficient of determination (R<sup>2</sup>), 381 and correlation coefficient (p). For example, sand prediction shows an RMSE of 9.322, an 382 R<sup>2</sup> of 0.841, and a correlation coefficient of 0.918. pH prediction shows an RMSE of 0.270, 383 an R<sup>2</sup> of 0.945, and a correlation coefficient of 0.972. These metrics are computed using 384 out-of-bag (OOB) samples from random forest regressors. OOB samples are data points 385 not included in the bootstrap samples used to train each tree in the random forest.





386 Additionally, these metrics are evaluated by comparing the expected values of posterior 387 predictions with co-located soil properties values; not computed on residuals. 388 389 Table 1 also shows variations in performance across different soil properties. SOM and 390 bulk density show slightly worse metrics compared to particle size fractions and pH. For instance, SOM predictions have an RMSE of 1.961, an R<sup>2</sup> of 0.608, and a correlation 391 coefficient of 0.801, and bulk density predictions have an RMSE of 0.164, an R<sup>2</sup> of 0.704, 392 393 and a correlation coefficient of 0.843. Two main reasons can result in their lower 394 performance. First, these properties are more dynamic in nature compared to particle size 395 fractions and pH. SOM and bulk density can change over time due to factors such as land 396 use practices. The prior predictions are trained using soil survey data that are older, while 397 the posterior soil profiles used for evaluation may come from a different period. Second, 398 SOM and bulk density are more challenging to model accurately. SOM is influenced by 399 complex biological and soil-forming processes, such as decomposition rates and organic 400 matter inputs. Similarly, bulk density is affected by soil compaction, organic matter 401 content, and soil structure. All of them can vary spatially and temporally. 402 Table 1: Performance metrics (RMSE, R<sup>2</sup>, and correlation coefficient ρ) for posterior 403 404 predictions of soil properties, including sand, silt, clay, pH, oven-dry bulk density 405 (BD), and soil organic matter (SOM). The table summarizes the range (minimum and 406 maximum values) and accuracy metrics for each property averaged across all depth 407 intervals.





Property	Unit	Min	Max	RMSE	R <sup>2</sup>	$\boldsymbol{\varphi}$
Sand	% mass	0.0	100.0	9.322	0.841	0.918
Silt	% mass	0.0	100.0	6.556	0.788	0.889
Clay	% mass	0.0	100.0	5.891	0.841	0.918
рН	log10([H <sup>+</sup> ])	3.0	10.0	0.270	0.945	0.972
BD (oven-dry)	g/cm³	0.5	2.0	0.164	0.704	0.843
SOM	% mass	0.0	100.0	1.961	0.608	0.801

The posterior predictions of soil properties all align with the co-located observations and can capture the general trend of observations (Figure 5). Predictions of pH show the most concentrated clustering to the dashed line, indicating good agreement with observations across all depths. SOM and bulk density show relatively weaker performance compared to other predicted soil properties. And this pattern of reduced accuracy persists throughout all depths.

As Figure 5 shows, the performance of the model tends to decline with increasing soil depth, except for SOM. This decline is primarily due to several reasons. First, the availability of soil data is often greater for shallower layers compared to deeper layers (such as > 1m), which limits the model's ability to learn patterns in deep layers. Second, remote sensing-derived soil covariates can only observe surface properties. Predictions





for deeper layers rely on soil horizon information, soil profiles, geology, and parent material-related features. The certainty and quantity of them are less than easily measurable surface covariates. However, SOM shows better performance in deeper layers compared to surface layers. This is likely because surface SOM is highly variable due to factors like residue, land use, and management practices, while deeper SOM tends to be more stable.

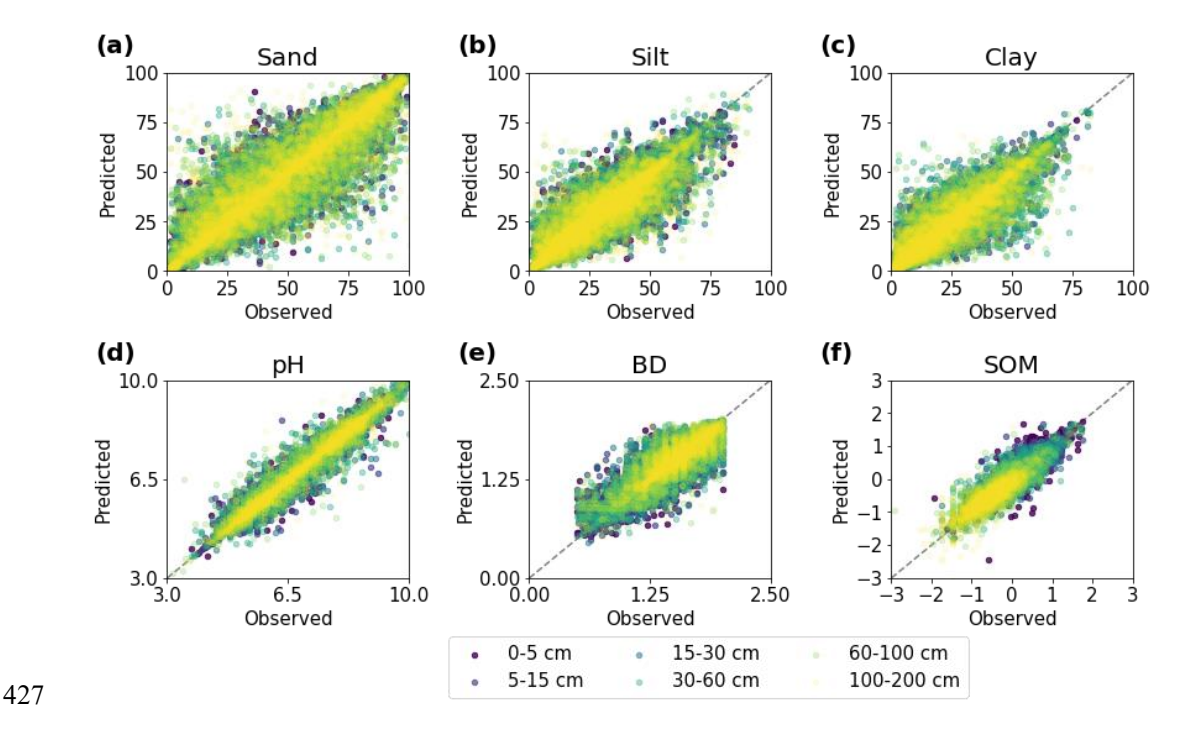


Figure 5: Evaluating posterior predictions with observations for six soil properties: (a) sand, (b) silt, (c) clay, (d) pH, (e) bulk density (BD), and (f) log-scaled soil organic matter (SOM). The left side shows scatter plots of posterior predictions versus observations across six depth intervals, with each depth represented by a distinct color. The dashed black line represents perfect prediction.



435

436

437

438

439

440

441

442

443

444

445

446

447

448

449

450

451

452

453

454

455

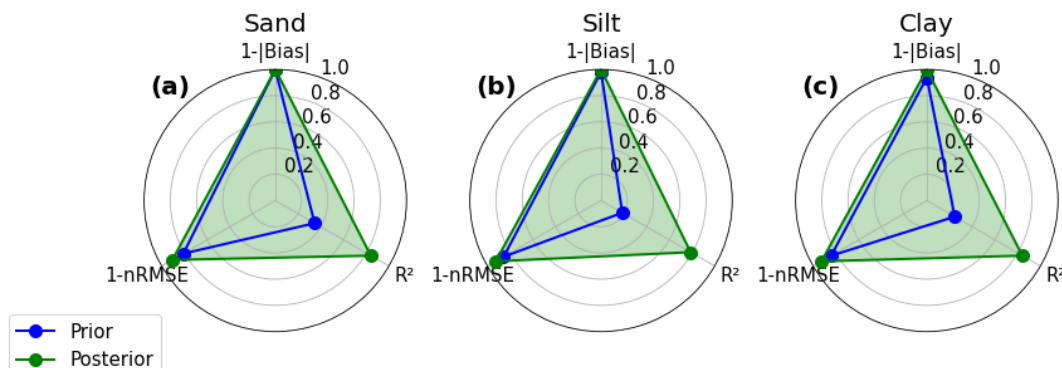


3.2 Comparison of Prior and Posterior Soil Predictions Prior and posterior predictions of soil properties are compared against co-located observations to assess the added value of residual correction. The radar plots in Figure 6 illustrate the improvements achieved through the residual correction method using three normalized metrics: 1-normalized absolute bias (1-|Bias|), coefficient of determination (R<sup>2</sup>), and 1-normalized RMSE by ranges of soil variability (1-nRMSE). These metrics are computed with values of soil properties, instead of on their residuals. Values in Figure 6 closer to the outer edge of each plot indicate better model performance. Overall, all soil properties maintain reasonable normalized bias, with nRMSE values consistently less than 0.02 for both prior and posterior predictions. However, the prior predictions tend to underestimate the variability of soil properties. As a result, the normalized metrics for prior and posterior predictions are similar, while the R<sup>2</sup> values show some differences. For all soil properties, posterior predictions consistently outperform prior predictions across all metrics. For particle size fractions, R<sup>2</sup> values show the largest improvements: sand increases from 0.35 to 0.84, silt from 0.19 to 0.79, and clay from 0.25 to 0.84. The nRMSE metric also shows improvements. Sand decreases from 0.19 to 0.09, silt from 0.14 to 0.07, and clay from 0.16 to 0.07, showing reductions in prediction errors using the residual correction. Figure 6 also shows different degrees of improvement across different soil properties. Prior pH predictions already demonstrate reasonable accuracy, with an R<sup>2</sup> of 0.54 and nRMSE of





0.11. After the residual correction, these metrics improve to 0.94 for  $R^2$  and 0.04 for nRMSE. Bulk density and SOM show the biggest gains. For bulk density, the  $R^2$  increasing from 0.16 to 0.70 and nRMSE reducing from 0.18 to 0.11. Prior SOM are underfitted with a low  $R^2$  value. With the residual correction, the posterior SOM show a positive  $R^2$  of 0.61. The nRMSE for SOM also improves from 0.07 to 0.04.



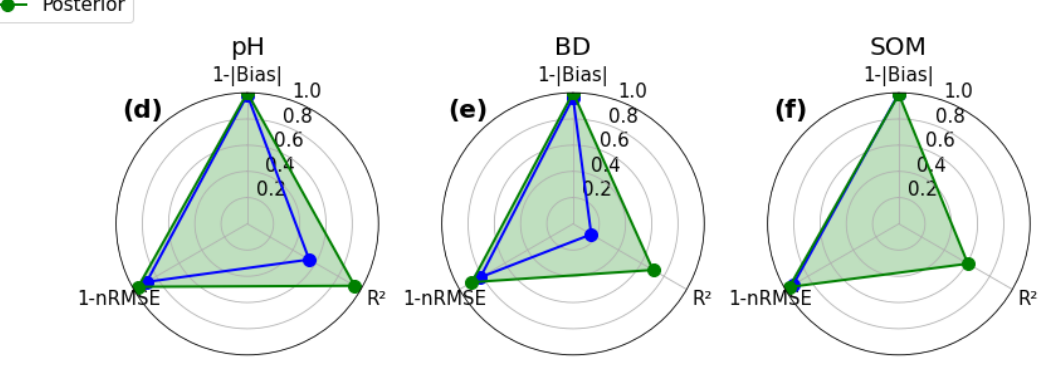


Figure 6: Radar plots comparing the performance metrics of prior and posterior predictions for six soil properties: (a) sand, (b) silt, (c) clay, (d) pH, (e) oven-dry bulk density (BD), and (f) soil organic matter (SOM). Each plot presents three metrics: 1-normalized absolute bias (1-|Bias|), coefficient of determination (R²), and 1-normalized RMSE by ranges of soil variability (1-nRMSE). Prior predictions are shown in blue, and posterior predictions in green. All metrics are scaled from 0 to 1, where





468 values closer to the outer edge of the plot indicate better model performance. The 469 green shaded area highlights the improvement achieved by the posterior predictions 470 over prior estimates. 471 472 Horizontal spatial patterns of the six soil properties are presented in Figure 7. In the 473 Central Valley California, soils are mostly medium textured with about 30% silt and lower 474 sand content compared to surrounding areas. In the Mojave and Colorado Deserts, high 475 sand contents (> 60%) with low clay contents are observed. SOM contents are also low in 476 these areas. The histograms show how residual correction adjusts the distribution of soil 477 properties. 478 479 For SOM and bulk density, the prior predictions often underestimate the observed 480 variation. Figure 7 shows that the residual correction processes add noticeable spatial 481 variations between prior and posterior soil maps. Prior bulk density values are often 482 clustered around 1.5 g/cm<sup>3</sup>, whereas the posterior histogram presents a broader range, spanning from 1.25 g/cm<sup>3</sup> to 1.6 g/cm<sup>3</sup>, capturing more heterogeneity of bulk density. 483 484 Similarly, the residual correction adds soil heterogeneity to SOM. The posterior SOM can 485 delineate water bodies, where SOM content is abruptly lower than the surrounding areas. 486 Additionally, the posterior SOM maps present hill features in the desert areas.





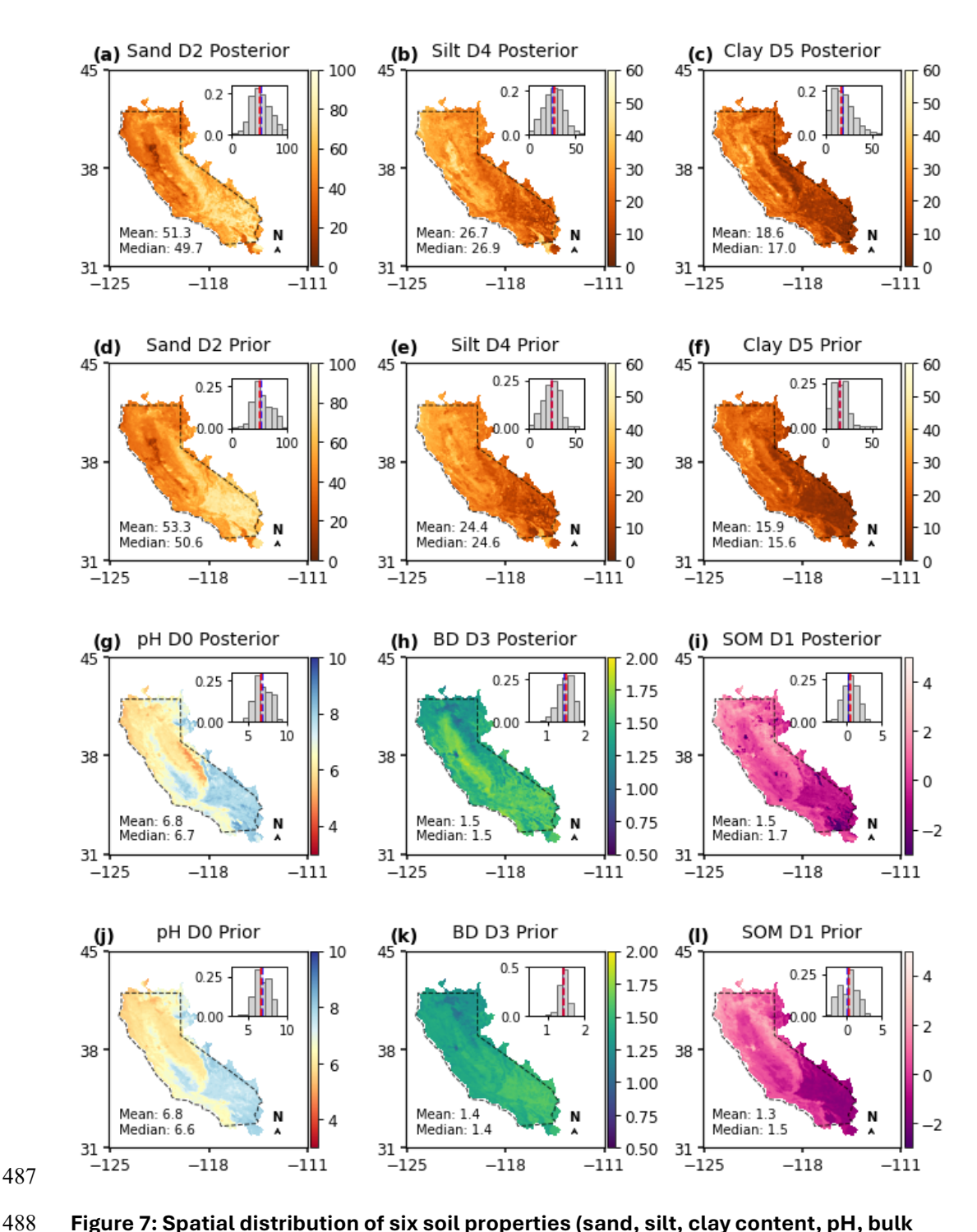


Figure 7: Spatial distribution of six soil properties (sand, silt, clay content, pH, bulk





490

491

492

493

494

495

496

497

498

499

500

501

502

503

504

505

506

507

508

509

density, and soil organic matter) across California. Maps of prior and posterior soil properties are compared. The corresponding frequency distributions of these soil properties are displayed in the right corner. Dashed polygons represent the continental part of California. In the histograms, the blue and red dashed lines represent the mean and median values, respectively. The maps labeled D0 to D5 correspond to the first vertical layer down to the deepest layer. Note the map and distribution of soil organic matter (SOM) is log-scaled. Mean and median values are computed from the original SOM data. Soil profiles used for evaluating residual correction are grouped according to their corresponding pixel's land use classification from the National Land Cover Database (NLCD). Figure 8 presents selected vertical soil profiles of sand content, oven-dry bulk density, and SOM across three land use categories: forest, cultivated crops, and wetland. The number of samples varies by land use, with forests having the most, cultivated crops approximately half as many, and wetlands the fewest across California. To ensure a balanced visualization, a similar number of profiles are selected from each category. Sand content is chosen due to its broader range of variation (0-100%) compared to silt and clay (< 60% range). SOM and bulk density, which show relatively lower performance metrics, are included to assess the model's 'lower-bound performance'. These vertical profiles were not used during model training.





511

512

513

514

515

516

517

518

519

520

521

522

523

524

525

526

527

528

529

530

531

In Figure 8, solid lines represent the mean soil profiles for sand content, oven-dry bulk density, and SOM across forest, cultivated crops, and wetland land use categories. Blue lines, red lines, and green lines indicate prior, observation, and posterior predictions. Comparing the solid lines, the posterior predictions align more closely with the observed data compared to the prior estimates. However, the degree of alignment varies by soil property. For sand content and SOM, the posterior predictions show better agreement with observations, while bulk density predictions exhibit greater discrepancies, particularly in cultivated areas. For sand content, the residual correction process improves estimates, especially in wetlands, with RMSE decreasing from 7.68 to 0.77 (%). Bulk density predictions perform better in forested and wetland areas. In cultivated crops, the posterior predictions show larger discrepancies. This suggests that bulk density is more challenging to predict in agricultural lands, particularly in shallow layers, likely due to agricultural activities. For SOM, the residual correction effectively improves estimates, especially in the surface layers of wetlands. Dashed lines in Figure 8 represent individual soil profiles. Prior predictions often underestimated the variability in soil properties, struggling to capture extreme values. After the residual correction, the posterior predictions are better able to approximate these extremes. However, the correction process sometimes introduces additional noise. For example, some low SOM values (such as 0.001 g/cm<sup>3</sup>) were generated during residual

https://doi.org/10.5194/egusphere-2025-5107 Preprint. Discussion started: 21 November 2025 © Author(s) 2025. CC BY 4.0 License.

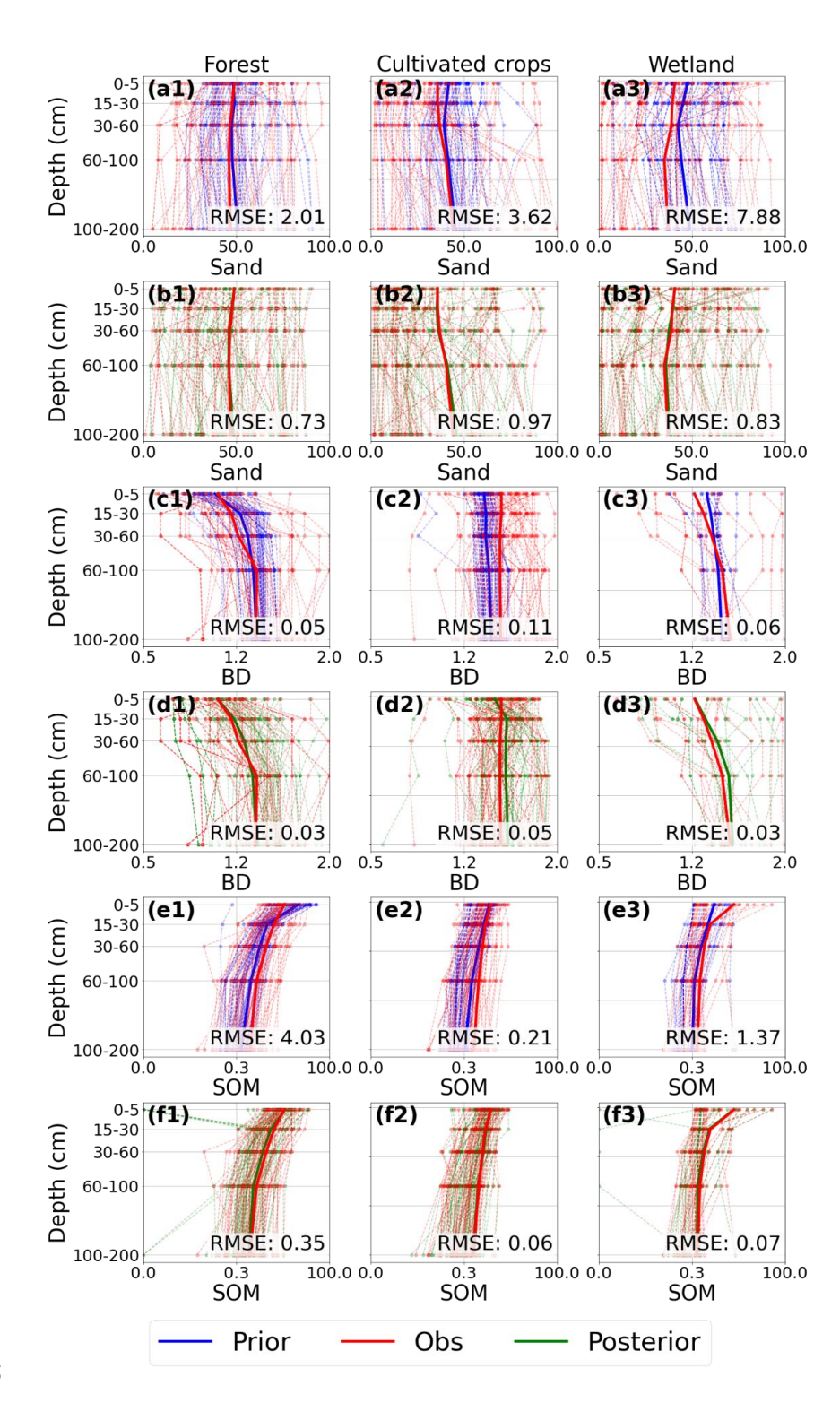




- 532 correction, even though such values are not presented in the observed data. It is likely due
- 533 to that we used the van Bemmelen factor (1.724) to convert the prior soil organic matter to
- 534 soil organic carbon.











537

538

539

540

541

542

543

544

545

546

547

548

549

550

551

552

553

554

555

556

557

Figure 8: Vertical distribution of soil properties (sand content, oven-dry bulk density, and soil organic matter SOM) across three land use categories: forest, cultivated crops, and wetland. Prior estimates (blue), posterior estimates (green), and observations (red) are shown as depth profiles. Dashed lines represent individual measurements, and solid lines show mean values. RMSE is computed elementwise to evaluate model performance across all depths. X-axis and Y-axis represent value ranges of a soil property and vertical depth intervals, respectively. 3.3 Uncertainty Analysis Figure 9 shows the differences between 5% — 95% posterior and prior prediction interval widths (PIWs) for six soil properties—sand, silt, clay, pH, bulk density, and SOM—from surface to 2-m deep. The differences are calculated by subtracting the prior PIWs from the posteriors. Red areas present a reduction in posterior PIW, indicating the residual correction has reduced uncertainties of soil properties predictions. Blue pixels suggest the opposite. White areas represent regions where the prior and posterior uncertainties are similar. In Figure 9, most pixels show reduced uncertainty for sand content after residual correction, particularly in agricultural and desert regions. This improvement is attributed to the inclusion of additional soil profile data from these areas. For clay content, the posterior predictions consistently show reduced uncertainty across the Sierra Nevada Mountain ranges. For SOM, the posterior PIWs improved in shallower layers (0-15 cm) over both the

https://doi.org/10.5194/egusphere-2025-5107 Preprint. Discussion started: 21 November 2025 © Author(s) 2025. CC BY 4.0 License.





Coastal Ranges and the Sierra Nevada Mountains, with the coastal line showing notably
narrower PIWs. For pH, the results present a mixed pattern of PIWs after residual
correction, with some areas showing reduced uncertainty and others showing the
opposite. Similarly, bulk density exhibits a mixed pattern, though deeper layers (60 cm to 2
m) generally show reduced uncertainty in the Central Valley, California.



564

565

566



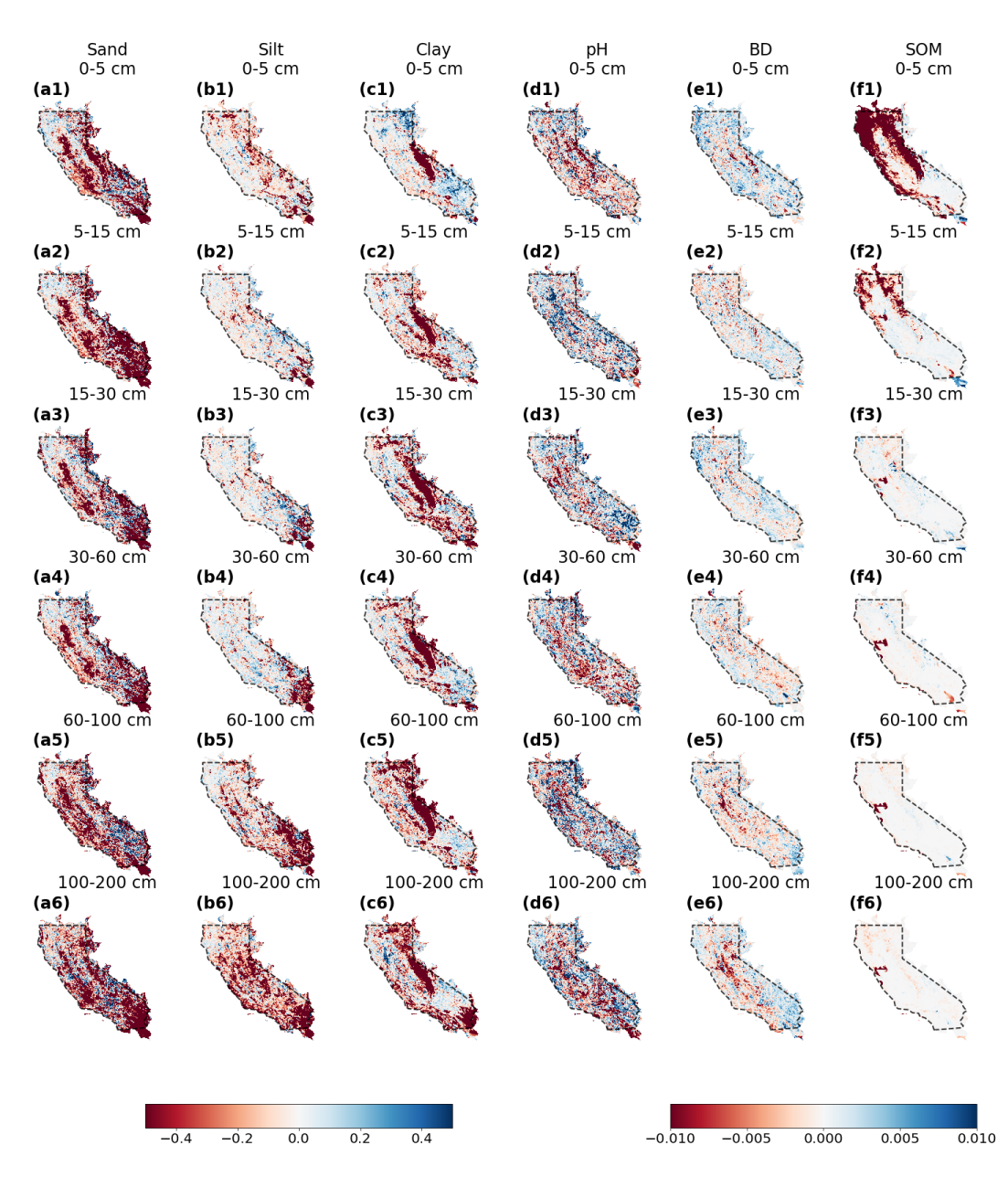


Figure 9: Differences of 5% — 95% posterior and prior prediction interval widths (PIWs) for soil properties across different depths. Each column represents a specific soil property and rows show different depths. Black polygons represent the continental part of California. Differences between posterior and prior PIWs are in a red-to-blue





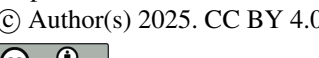
color scale. Red pixels indicate a decrease in posterior PIW, indicating residual correction reduces uncertainties. Vice versa for blue pixels. White areas indicate similar extent of uncertainties. The left colorbar corresponds to sand, silt, clay with wider ranges of PIW differences. The right colorbar represents other properties with smaller PIW changes.

#### 4 Discussion

### 4.1 Limitations in Soil Profile Data

The effectiveness of residual correction depends on the spatial and vertical distribution of soil profiles used to calculate residuals. In regions with sparse sampling, such as California's desert areas (Figure 1), the limited number of profiles leads to interpolating the entire area using limited observations. If soil heterogeneity is not captured by these limited samples, the residual correction would overlook it. For soil texture, most data collected by staff working on multiple projects under the National Institute of Food and Agriculture (NIFA) and the Sustainable Agricultural Systems (SAS) programs range from the surface to 1.1 meters deep (additional field measurements used in this work). We use spline interpolation to predict soil texture data beyond 1.1-m depths. It assumes vertical continuity in soil properties, which may not reflect abrupt changes in subsurface layers.

Uncertainty also arises from converting some soil organic carbon (SOC) data to soil organic matter (SOM). We used the van Bemmelen factor (1.724) to convert SOC to SOM profiles. This factor does not hold true in scenarios such as organic-rich soils. Adding data



591

592

593

594

595

596

597

598

599

600

601

602

603

604

605

606

607

608

609

610



quality controls—such as filtering profiles based on metadata (such as soil type, land use)—could filter out samples that are not suitable for this conversion. However, this conversion still has uncertainties, since even for mineral soils, this factor still has a certain extent of variation depending on the organic matter composition (lower for soils with more decomposed organic matter), soil types (forest soils or wetland soils with anaerobic decomposition), and environmental influences (such as microbial activity).

## 4.2 Computational Challenges

The iterative residual correction process on distributions requires computational resources, particularly when applied to large-extent or high-resolution datasets. This process involves adjusting multiple values for each pixel, as each pixel represents a distribution of soil properties. This process can be approached in two ways. The first method involves correcting the residual values for each pixel, adding these residuals to update the posterior values of soil properties, and then converting these updated values to generate a posterior distribution of soil properties. The second method first converts all pixel values into the same histogram bins and then corrects the shape of these histogram bins for each pixel. Thus, the number of values retained per pixel affects computational expense. Based on our experience, using method two, especially for soil texture, requires 100-bin histograms. Using method one with 20 most probable prior property values for residual correction can achieve comparable results while reducing memory usage.





612

613

614

615

616

617

618

619

620

621

622

623

624

625

626

627

628

629

630

631

The iterative process of updating features and correcting residuals also plays a role. In our simulations, we observed that subsequent residual corrections generally align with previous ones. To ensure consistency, we require the corrections to converge more than three times across different depths. For example, residual correction for a 1-km soil property map over California takes approximately two hours after preprocessing the input data. However, processing higher-resolution datasets, such as those at a 10-meter scale, can demand significantly more computational resources. This highlights the trade-off between resolution and computational efficiency in DSM projects. 4.3 Temporal and Spatial Constraints The current method does not account for temporal changes in soil properties, limiting its applicability to dynamic properties like soil organic matter or bulk density. Incorporating temporal covariates (such as seasonal land surface temperature, recent land-use changes) or stratifying soil profiles by collection date could address this. However, such improvements rely on the availability of temporally resolved soil data, which are often limited in quantities and sampling frequency. Spatial clustering of soil samples poses another challenge. While duplicate profiles were removed during data preprocessing, nearby samples may still share a certain level of similarity due to spatial autocorrelation. This could lead to overly optimistic evaluation of

residual correction performance. Two methods can help address this issue:





632 (1) Cross-validation with spatial considerations: Implement a cross-validation 633 method for splitting training and validation sets with attention to sample locations. 634 Ensure a minimum distance between training samples and evaluation data. 635 636 (2) Independent dataset evaluation: Use independent datasets to evaluate the 637 model. CONUS-wide instrumental network, such as the U.S. Climate Reference 638 Network and the National Ecological Observatory Network, provide independent 639 soil data. However, these datasets have limitations as they were collected with 640 clustering to certain landscapes, potentially introducing bias in the evaluation. 641 642 4.4 Similar Studies 643 Several continental-scale DSM products (or methods) are compared, including the Soil 644 Survey Geographic Database (SSURGO), the Gridded National Soil Survey Geographic 645 Database (gNATSGO), the Probabilistic Layers for the Assessment of Soils (POLARIS), Soil-646 Landscape Unified Synthesis (SOLUS), and the pruned Hierarchical Random Forest with 647 iterative bias correction (pHRF with IRC) soil properties. SSURGO is a traditional, polygon-648 based product derived from expert field surveys and remains widely used in agricultural 649 applications (Soil Survey Staff et al., 2023), gNATSGO mainly builds on SSURGO by 650 rasterizing its map units to improve spatial coverage. And its estimation of soil properties 651 still rely on utilizing metadata of legacy soil data (Soil survey staff, 2023). These two still 652 inherit legacy data's limitations, such as scale inconsistency between soil map units and

derived soil maps, inconsistencies with field observations, and report distribution of soil





654 properties with only three values (low end value, representative value, and high end value) 655 (Rossiter et al., 2022; Soil Survey Staff, 2025; Xu et al., 2025). 656 657 Development of the following DSM products incorporates quantitative models in their 658 methodology. POLARIS produces probabilistic soil property maps using machine learning 659 and the DSMART algorithm (Chaney et al., 2016, 2019; Odgers et al., 2015), while the 660 uncertainties in the DSMART algorithm can propagate into POLARIS. SOLUS integrates 661 legacy soil data with georeferenced field observations and employs linear adjusted 662 Random Forest to predict soil properties (Nauman et al., 2024). SOLUS hierarchizes soil 663 data with different qualities into its training dataset, giving more attention to georeferenced 664 observations. However, since it also uses resampled soil data derived from polygon-based 665 soil map units, this process may introduce additional uncertainties into the final product. 666 The pHRF with IRC follows a different approach. Unlike most DSM methods that directly 667 predict soil properties from input data, this approach works in two steps: first, it generates 668 a prior estimate of soil taxa and property values, then iteratively adjusts these estimates to 669 improve model performance. In future work, the pHRF with IRC method will be applied on 670 large scale and assessed with more soil properties to evaluate its generalizability. 671 672 5 Conclusion 673 The study introduces an iterative residual correction method for post processing used in a 674 Digital Soil Mapping (DSM) framework. The method integrates additional soil profile data 675 and iteratively optimizes the feature space to refine the distribution of soil properties until





677

678

679

680

681

682

683

684

685

686

687

688

689

690

691

692

693

694

695

696

697

the residual correction model converges. Convergence is achieved when the median difference between updated and previous predictions falls below a predefined threshold, ensuring consistent predictions. The proposed DSM method operates through two primary steps: (1) generating prior soil property maps using the pruned hierarchical Random Forest (pHRF) approach, and (2) performing iterative residual correction on the priors. Residuals (differences between observed values and prior predictions) are calculated and added to the prior distributions to adjust the statistical shape of the probability distribution pixel-bypixel. The feature space, which includes soil covariates, depth information, and vertical correlations, is iteratively optimized to capture incremental adjustments to subsequent predictions. Using this method, we updated posterior distribution of soil properties for sand, silt, clay content, soil pH, oven-dry bulk density, and soil organic matter over California. The results show improvements in the accuracy of soil properties predictions, as shown by multiple metrics including RMSE, R<sup>2</sup>, and correlation coefficients. Furthermore, the iterative residual correction model reduced prediction uncertainties, presenting narrower prediction intervals compared to the priors. Several innovations contribute to the method's improvements. First, the integration of additional soil profiles allows the model to further learn from georeferenced soil information, complementing prior soil property estimates derived from traditional surveys. Second, the iterative optimization of feature space captures both spatial and





vertical soil heterogeneity through a carefully selected combination of soil covariates and vertical correlations among soil profile observations. Third, the convergence-based approach to residual correction ensures stable output of posterior predictions while avoiding overfitting since only converged residuals are added to the priors. Fourth, the implementation of physical constraints and compositional data handling maintains the realism of predicted soil properties. Future research could explore the application of this framework to other soil properties and environmental contexts, such as soil hydraulic properties and CONUS-wide simulation, to test the framework's generalization, supporting informed decision-making in soil-related applications.

## Data Availability

Data will be made available on request.

#### **Author Contributions**

Chengcheng Xu and Nathaniel Chaney designed the study and developed the methodology. Chengcheng Xu wrote the original draft and wrote the codes to produce the methodology and analyses. Nathaniel Chaney supervised the work, provided resources and funding, and helped guide the research direction. Elia Schudiero and Ray Anderson provided soil property samples from California that were used as part of the input dataset. Chengcheng Xu, Nathaniel Chaney, Elia Schudiero, and Ray Anderson discussed the results and contributed to revising and editing the manuscript.





# **Competing Interests**

721 The authors declare that they have no conflict of interest.

**Acknowledgements** 

This study was supported by USDA-NIFA-AFRI-006739 grant for sustainable agricultural systems. The authors want to thank Dr. Todd Skaggs for his and his teams' support for gathering input data for this work. His and Dr. Ray Anderson's efforts are supported by USDA-ARS, Office of National Programs (projects 2036-61000-019-000-D and 2036-61000-019-006-R). The U.S. Department of Agriculture prohibits discrimination in all its programs and activities on the basis of race, color, national origin, age, disability, and where applicable, sex, marital status, familial status, parental status, religion, sexual orientation, genetic information, political beliefs, reprisal, or because all or part of an individual's income is derived from any public assistance program (not all prohibited bases apply to all programs). Persons with disabilities who require alternative means for communication of program information (braille, large print, audiotape, etc.) should contact USDA's TARGET Center at (202) 720-2600 (voice and TDD). To file a complaint of discrimination, write to USDA, Director, Office of Civil Rights, 1400 Independence Avenue, S.W., Washington, D.C. 20250-9410, or call (800) 795-3272 (voice) or (202) 720-6382 (TDD). USDA is an equal opportunity provider and employer.





## 740 Financial Support

- 741 The study was supported by USDA-NIFA-AFRI-006739 grant for sustainable agricultural
- 742 systems.

743

744

#### References

- 745 Batjes, N. H., Calisto, L., and de Sousa, L. M.: Providing quality-assessed and standardised
- 746 soil data to support global mapping and modelling (WoSIS snapshot 2023), Earth System
- 747 Science Data, 16, 4735–4765, https://doi.org/10.5194/essd-16-4735-2024, 2024.
- 748 Chaney, N. W., Wood, E. F., McBratney, A. B., Hempel, J. W., Nauman, T. W., Brungard, C.
- 749 W., and Odgers, N. P.: POLARIS: A 30-meter probabilistic soil series map of the contiguous
- 750 United States, Geoderma, https://doi.org/10.1016/j.geoderma.2016.03.025, 2016.
- 751 Chaney, N. W., Minasny, B., Herman, J. D., Nauman, T. W., Brungard, C. W., Morgan, C. L.
- 752 S., McBratney, A. B., Wood, E. F., and Yimam, Y.: POLARIS Soil Properties: 30-m
- 753 Probabilistic Maps of Soil Properties Over the Contiguous United States, Water Resources
- 754 Research, https://doi.org/10.1029/2018WR022797, 2019.
- 755 Chen, C., Liaw, A., and Breiman, L.: Using random forest to learn imbalanced data,
- 756 University of California, Berkeley, 110, 24, 2004.
- 757 Chilès, J.-P. and Delfiner, P.: Geostatistics: modeling spatial uncertainty, in: Geostatistics:
- 758 modeling spatial uncertainty, John Wiley & Sons, Ltd, 147–237,
- 759 https://doi.org/10.1002/9781118136188.ch3, 2012.
- 760 Corwin, D. L. and Scudiero, E.: Field-scale apparent soil electrical conductivity, Soil
- 761 Science Society of America Journal, 84, 1405–1441, https://doi.org/10.1002/saj2.20153,
- 762 2020.
- 763 Grunwald, S., Thompson, J. A., and Boettinger, J. L.: Digital Soil Mapping and Modeling at
- 764 Continental Scales: Finding Solutions for Global Issues, Soil Science Society of America
- 765 Journal, 75, 1201–1213, https://doi.org/10.2136/SSSAJ2011.0025, 2011.
- 766 Haghverdi, A., Najarchi, M., öztürk, H. S., and Durner, W.: Studying unimodal, bimodal, PDI
- 767 and bimodal-PDI variants of multiple soil water retention models: I. Direct model fit using
- the extended evaporation and dewpoint methods, Water (Switzerland), 12,
- 769 https://doi.org/10.3390/w12030900, 2020.
- 770 Hengl, T., Heuvelink, G. B., and Stein, A.: A generic framework for spatial prediction of soil
- variables based on regression-kriging, Geoderma, 120, 75–93, 2004.





- Hengl, T., De Jesus, J. M., Heuvelink, G. B. M., Gonzalez, M. R., Kilibarda, M., Blagotić, A.,
- 773 Shangguan, W., Wright, M. N., Geng, X., Bauer-Marschallinger, B., Guevara, M. A., Vargas,
- 774 R., MacMillan, R. A., Batjes, N. H., Leenaars, J. G. B., Ribeiro, E., Wheeler, I., Mantel, S.,
- 775 and Kempen, B.: SoilGrids250m: Global gridded soil information based on machine
- 776 learning, PLoS ONE, https://doi.org/10.1371/journal.pone.0169748, 2017.
- Jiang, Q., Fu, Q., and Wang, Z.: Delineating site-specific irrigation management zones,
- 778 Irrigation and Drainage, 60, 464–472, https://doi.org/10.1002/ird.588, 2011.
- Lesch, S., Rhoades, J., and Corwin, D.: ESAP-95 version 2.01 R: User manual and tutorial
- 780 guide, Research Rpt, 146, 17, 2000.
- 781 Lesch, S. M.: Sensor-directed response surface sampling designs for characterizing spatial
- 782 variation in soil properties, Computers and Electronics in Agriculture, 46, 153–179,
- 783 https://doi.org/10.1016/j.compag.2004.11.004, 2005.
- 784 Li, N., Zhao, X., Wang, J., Sefton, M., and Triantafilis, J.: Digital soil mapping based site-
- 785 specific nutrient management in a sugarcane field in Burdekin, Geoderma, 340, 38–48,
- 786 https://doi.org/10.1016/j.geoderma.2018.12.033, 2019.
- 787 Minasny, B. and McBratney, A. B.: A conditioned Latin hypercube method for sampling in
- 788 the presence of ancillary information, Computers & geosciences, 32, 1378–1388, 2006.
- 789 Mueller, T. G., Pierce, F. J., Schabenberger, O., and Warncke, D. D.: Map Quality for Site-
- 790 Specific Fertility Management, Soil Science Society of America Journal, 65, 1547–1558,
- 791 https://doi.org/10.2136/sssaj2001.6551547x, 2001.
- 792 National Cooperative Soil Survey: NCSS Soil Characterization Database (Lab Data Mart),
- 793 2018.
- Nauman, T. W., Kienast-Brown, S., Roecker, S. M., Brungard, C., White, D., Philippe, J., and
- 795 Thompson, J. A.: Soil landscapes of the United States (SOLUS): Developing predictive soil
- 796 property maps of the conterminous United States using hybrid training sets, Soil Science
- 797 Society of America Journal, 88, 2046–2065, https://doi.org/10.1002/saj2.20769, 2024.
- 798 Nussbaum, M., Zimmermann, S., Walthert, L., and Baltensweiler, A.: Benefits of
- 799 hierarchical predictions for digital soil mapping—An approach to map bimodal soil pH,
- 800 Geoderma, 437, 116579, https://doi.org/10.1016/j.geoderma.2023.116579, 2023.
- 801 Odgers, N. P., McBratney, A. B., and Minasny, B.: Digital soil property mapping and
- 802 uncertainty estimation using soil class probability rasters, Geoderma, 237,
- 803 https://doi.org/10.1016/j.geoderma.2014.09.009, 2015.
- 804 Oliver, M. A. and Webster, R.: A tutorial guide to geostatistics: Computing and modelling
- variograms and kriging, CATENA, 113, 56–69,
- 806 https://doi.org/10.1016/j.catena.2013.09.006, 2014.





- Ortuani, B., Chiaradia, E. A., Priori, S., L'Abate, G., Canone, D., Comunian, A., Giudici, M.,
- 808 Mele, M., and Facchi, A.: Mapping Soil Water Capacity Through EMI Survey to Delineate
- 809 Site-Specific Management Units Within an Irrigated Field, Soil Science, 181, 252,
- 810 https://doi.org/10.1097/SS.000000000000159, 2016.
- 811 Poggio, L., De Sousa, L. M., Batjes, N. H., Heuvelink, G. B. M., Kempen, B., Ribeiro, E., and
- 812 Rossiter, D.: SoilGrids 2.0: Producing soil information for the globe with quantified spatial
- 813 uncertainty, SOIL, 7, 217–240, https://doi.org/10.5194/SOIL-7-217-2021, 2021.
- 814 Powers, J. S., Corre, M. D., Twine, T. E., and Veldkamp, E.: Geographic bias of field
- 815 observations of soil carbon stocks with tropical land-use changes precludes spatial
- extrapolation, Proceedings of the National Academy of Sciences, 108, 6318–6322,
- 817 https://doi.org/10.1073/pnas.1016774108, 2011.
- 818 Ramcharan, A., Hengl, T., Nauman, T., Brungard, C., Waltman, S., Wills, S., and Thompson,
- 3.: Soil Property and Class Maps of the Conterminous United States at 100-Meter Spatial
- 820 Resolution, Soil Science Society of America Journal, 82, 186–201,
- 821 https://doi.org/10.2136/sssaj2017.04.0122, 2018.
- 822 Rossiter, D. G., Poggio, L., Beaudette, D., and Libohova, Z.: How well does digital soil
- 823 mapping represent soil geography? An investigation from the USA, SOIL, 8, 559-586,
- 824 https://doi.org/10.5194/soil-8-559-2022, 2022.
- 825 Schmidinger, J. and Heuvelink, G. B. M.: Validation of uncertainty predictions in digital soil
- 826 mapping, Geoderma, 437, 116585, https://doi.org/10.1016/j.geoderma.2023.116585,
- 827 2023.
- 828 Sharififar, A., Sarmadian, F., Malone, B. P., and Minasny, B.: Addressing the issue of digital
- 829 mapping of soil classes with imbalanced class observations, Geoderma, 350, 84–92,
- 830 https://doi.org/10.1016/j.geoderma.2019.05.016, 2019.
- 831 Shi, G., Sun, W., Shangguan, W., Wei, Z., Yuan, H., Zhang, Y., Liang, H., Li, L., Sun, X., Li, D.,
- 832 Huang, F., Li, Q., and Dai, Y.: A China dataset of soil properties for land surface modeling
- 833 (version 2), https://doi.org/10.5194/essd-2024-299, 29 August 2024.
- 834 Soil survey staff: Gridded National Soil Survey Geographic (gNATSGO) Database for the
- 835 Conterminous United States, 2023. Natural Resources Conservation Service, United
- 836 States Department of Agriculture.
- 837 Soil Survey Staff: Gridded Soil Survey Geographic (gSSURGO) Database for the
- 838 Conterminous United States, 2025. Natural Resources Conservation Service, United
- 839 States Department of Agriculture.
- 840 Soil Survey Staff, Natural Resources Conservation Service, and United States Department
- 841 of Agriculture: Soil Survey Geographic (SSURGO) Database for the CONUS, 2023. Natural
- Resources Conservation Service, United States Department of Agriculture.





- 843 Sylvain, J.-D., Anctil, F., and Thiffault, É.: Using bias correction and ensemble modelling for
- 844 predictive mapping and related uncertainty: A case study in digital soil mapping,
- 845 Geoderma, 403, 115153, https://doi.org/10.1016/j.geoderma.2021.115153, 2021.
- 846 Takoutsing, B., Heuvelink, G. B. M., Stoorvogel, J. J., Shepherd, K. D., and Aynekulu, E.:
- 847 Accounting for analytical and proximal soil sensing errors in digital soil mapping, European
- 848 Journal of Soil Science, 73, e13226, https://doi.org/10.1111/ejss.13226, 2022.
- Vereecken, H., Schnepf, A., Hopmans, J. W., Javaux, M., Or, D., Roose, T., Vanderborght, J.,
- Young, M. H., Amelung, W., Aitkenhead, M., Allison, S. D., Assouline, S., Baveye, P., Berli,
- 851 M., Brüggemann, N., Finke, P., Flury, M., Gaiser, T., Govers, G., Ghezzehei, T., Hallett, P.,
- Hendricks Franssen, H. J., Heppell, J., Horn, R., Huisman, J. A., Jacques, D., Jonard, F.,
- 853 Kollet, S., Lafolie, F., Lamorski, K., Leitner, D., McBratney, A., Minasny, B., Montzka, C.,
- Nowak, W., Pachepsky, Y., Padarian, J., Romano, N., Roth, K., Rothfuss, Y., Rowe, E. C.,
- 855 Schwen, A., Šimůnek, J., Tiktak, A., Van Dam, J., van der Zee, S. E. A. T. M., Vogel, H. J.,
- 856 Vrugt, J. A., Wöhling, T., and Young, I. M.: Modeling Soil Processes: Review, Key
- 857 Challenges, and New Perspectives, Vadose Zone Journal, 15, vzj2015.09.0131,
- 858 https://doi.org/10.2136/vzj2015.09.0131, 2016.
- Vereecken, H., Amelung, W., Bauke, S. L., Bogena, H., Brüggemann, N., Montzka, C.,
- 860 Vanderborght, J., Bechtold, M., Blöschl, G., Carminati, A., Javaux, M., Konings, A. G.,
- 861 Kusche, J., Neuweiler, I., Or, D., Steele-Dunne, S., Verhoef, A., Young, M., and Zhang, Y.:
- 862 Soil hydrology in the Earth system, Nat Rev Earth Environ, 3, 573–587,
- 863 https://doi.org/10.1038/s43017-022-00324-6, 2022.
- 864 Wu, Y., Huang, Y., Chen, Z., Yao, Z., Fu, Y., Liu, K., Luo, X., and Wang, D.: Iterative Feature
- 865 Space Optimization through Incremental Adaptive Evaluation,
- 866 https://doi.org/10.48550/arXiv.2501.14889, 24 January 2025.
- Xu, C., Huang, J., Hartemink, A. E., and Chaney, N. W.: Pruned hierarchical Random Forest
- 868 framework for digital soil mapping: Evaluation using NEON soil properties, Geoderma, 459,
- 869 117392, https://doi.org/10.1016/j.geoderma.2025.117392, 2025.
- 870 Zhang, G. and Lu, Y.: Bias-corrected random forests in regression, Journal of Applied
- 871 Statistics, 39, 151–160, https://doi.org/10.1080/02664763.2011.578621, 2012.